



Antibacterial property of graphene quantum dots-modified TiO₂ nanorods on titanium dental implant

Xiang-yu ZHANG¹, Shu-xin LU², Dong-mei HE², Mao-zhou CHAI¹,
Zhuang-zhuang WU³, Xiao-hong YAO², Yong-qiang YANG⁴

1. College of Biomedical Engineering, Taiyuan University of Technology, Taiyuan 030024, China;

2. Shanxi Key Laboratory of Biomedical Metal Materials, College of Materials Science and Engineering, Taiyuan University of Technology, Taiyuan 030024, China;

3. Shanxi Key Laboratory of Bone and Soft Tissue Injury Repair, Department of Orthopedics, Second Hospital of Shanxi Medical University, Taiyuan 030001, China;

4. Special Equipment Safety Supervision Inspection Institute of Jiangsu Province, National Graphene Products Quality Inspection and Testing Center (Jiangsu), Wuxi 214174, China

Received 7 February 2022; accepted 27 May 2022

Abstract: Graphene quantum dots (GQDs) were incorporated into TiO₂ nanorods (TiO₂NR) by hydrothermal treatment to prevent bacterial infections of Ti implants. The successful preparation of TiO₂NR doped with GQDs on Ti was confirmed by scanning electron microscopy, high-resolution transmission electron microscopy, atomic force microscopy, X-ray photoelectron spectroscopy, X-ray diffraction and Fourier transform infrared spectrometer. Results showed that the mean diameter of the nanorod was 60 nm, and the hydrophilicity was significantly improved. The GQDs-modified TiO₂NR showed excellent antimicrobial effect against *Streptococcus mutans* with an efficiency of 97.8% due to the combined effect of GQDs and nanorod structure. Moreover, GQDs-modified TiO₂NR exhibited good biocompatibility and osteogenetic potency for cell spreading, thus contributing to the new bone formation even in bacteria-induced implant infection.

Key words: graphene quantum dots; nanorod; titanium; antibacterial property; osseointegration

1 Introduction

The demand for dental implants is growing worldwide as the population ages. Titanium (Ti) and its alloys are widely applied in dentistry appliances due to their mechanical performance, corrosion resistance and biocompatibility [1–3]. However, Ti dental implant-associated infections induced by *Streptococcus mutans* (*S. mutans*) delay the healing process and require long-term systemic antibiotic therapy [4,5]. Unfortunately, the abuse of antibiotics increases subinhibitory concentrations to

bacteria, which drives the bacteria toward drug resistance, as explained by the spreading of multidrug-resistant bacteria [6–8]. Therefore, new and effective means to prevent implant-associated bacterial infections must be explored.

Over the past two decades, investigators have attempted to address the implant-associated infections by surface modification or changing topological features. Organic (chitosan, polypeptide, etc) and inorganic (Ag, Cu, Zn, etc) antimicrobial agents were introduced onto the surface of Ti to kill bacteria [9–11], while the poor long-term performance of organic antimicrobial agents

and the toxicity of metal ions limit their clinical applications. Various nanostructured surfaces were also fabricated on implants to prevent bacterial infections by physical puncture [12–15]. Although the strategy is safer and more sustainable, and the nanostructure may promote cell differentiation and induce bone regeneration, the antibacterial activity is too low to fulfil practical requirement. Recently, light-assisted antibacterial therapy has attracted much attention due to the high antibacterial activity [16–20]. While whether photodynamic or photothermal therapy needs photosensitizer to absorb and convert light energy, the long-term safety of the light-sensitive material remains a significant challenge.

Graphene and its derivative, as the two-dimensional carbon-based nanoparticles, have attracted wide attention in various biomedical applications, such as precise biosensing and drug delivery, due to their biocompatibility, ease of functionalization and high surface area [21–23]. As is well-known, graphene-based nanomaterials also possess antibacterial property and have been introduced on the surface of polymers and metallic materials [24,25] to exert antibacterial effects. Moreover, graphene has also been reported to promote cell adhesion and enhance osseointegration of implants [26,27].

In this work, a synergetic antibacterial modality based on the sterilization by combining graphene quantum dots (GQDs) and TiO_2 nanostructures was proposed. To the best of our knowledge, graphene quantum dots-modified TiO_2 nanorods (G- TiO_2 NR) were fabricated on Ti dental implant for the first time to prevent bacterial infections. We firstly synthesized histidine-functionalized GQDs by simple pyrolysis of citric acid and amino acid [28,29], and the histidine residue (imidazole group) remaining on the surface makes GQDs possess excellent antibacterial activity. Meanwhile, TiO_2 nanorods (TiO_2 NR) were prepared on the surface of Ti by a hydrothermal method [30,31]. Then, GQDs were doped into TiO_2 nanorods by the secondary hydrothermal treatment. G- TiO_2 NR showed excellent in vitro and in vivo antibacterial activity against *S. mutans* due to the combined effect of physical puncture by nanorod and GQDs. Besides, G- TiO_2 NR also promoted new bone formation in vivo even in the presence of infection.

2 Experimental

Citric acid and histidine were purchased from Shanghai Maclean Biochemical Co., Ltd. Hydrochloric acid (HCl) was purchased from Sinopharm Group Chemical Reagent Co., Ltd. Sodium hydroxide (NaOH) was obtained from Tianjin Guangfu Technology Development Co., Ltd. Fetal bovine serum (FBS), penicillin, streptomycin, acridine orange (AO), and propidium iodide (PI) were purchased from Shanghai Sanko Biotechnology Development Co., Ltd. Anhydrous ethanol was supplied by Tianjin Bohuatong Chemical Products Sales Centre. Acetone was obtained by Tianjin Shentai Chemical Reagent Co., Ltd. All reagents were not further purified and the experimental water was deionized water.

2.1 Preparation of G- TiO_2 NR

GQDs were synthesized according to the procedures described previously [28,29]. Briefly, citric acid was used as carbon precursor and histone acid was used as functional reagent. GQDs with a lot of histidine residues (imidazolyl) on the surface were prepared by a simple pyrolysis. TiO_2 nanorod was prepared also by using a reported method [30,31]. Ti foil was cleaned ultrasonically and then hydrothermally treated with NaOH solution in a reaction kettle. After ion exchange in HCl, TiO_2 nanorod was prepared on Ti by annealing.

10 mg of GQDs were added to a mixture of 10 mL of alcohol and 20 mL of deionized water, stirring to make GQDs uniformly disperse in the mixture. Subsequently, both the solution and TiO_2 NR were transferred to a reaction kettle, and after treating for 4 h at 140 °C, G- TiO_2 NR was prepared.

2.2 Characterization

The microstructure of GQDs and G- TiO_2 NR was analyzed by high-resolution transmission electron microscopy (HR-TEM, JEM-2100F, JEOL). The morphology of TiO_2 and G- TiO_2 NR was observed by field emission scanning electron microscopy (FE-SEM, JSM-7001F, JEOL) and atomic force microscopy (AFM, XE-100, Park Systems). The phase composition and chemical states of TiO_2 and G- TiO_2 NR were analyzed by X-ray diffraction (XRD, Rigaku Dmax-3C, $\text{Cu K}\alpha$

radiation) and X-ray photoelectron spectroscopy (XPS, K-Alpha, Thermo). Fourier transform infrared spectrometer (FTIR, ALPHA II, Bruker, Germany) was used to determine the surface functional groups of the samples. Contact angle instrument (JC2000D2, Powereach, China) was employed to evaluate the surface hydrophilicity of TiO₂ and G-TiO₂ NR.

2.3 In vitro antibacterial property evaluation

The in vitro antibacterial property against *S. mutans* was quantitatively evaluated by the spread plate technique. 50 µL bacterial suspension (1×10^7 CFU/mL) was inoculated on the samples. After 24 h incubation at 37 °C, the bacterial suspension was diluted 100 times and 50 µL of diluted suspension was spread on LB agar plates. The bacterial colonies were counted after 18 h incubation. The antimicrobial activity was also evaluated by live/dead fluorescent staining. 1 mL of bacterial suspension was seeded on the samples. After 24 h incubation, the bacteria were stained by acridine orange/propidium iodide for 15 min in darkness. Finally, the samples were examined by a confocal scanning laser microscope (CLSM, C2 Plus, Nikon).

2.4 In vitro biocompatibility evaluation

Bone marrow mesenchymal stem cells (BMSCs) extracted from the femoral and tibial bone marrow of a 4-week-old rat following protocol [32,33] were used to evaluate the biocompatibility of G-TiO₂ NR. The specific cultivation processes were performed as previously described in Ref. [34]. In short, the cells were incubated on the samples with a density of 2×10^4 cells/cm². After 24 h incubation, BMSCs were fixed with 4% paraformaldehyde for 30 min, and then stained with FITC-phalloidin and 4,6-diamidino-2-phenylindole (DAPI) in darkness, respectively. Four regions were randomly photographed by a CLSM.

2.5 In vivo antibacterial assay and osteogenesis evaluation

All animal surgical procedures were approved by the Animal Ethics Committee of Taiyuan University of Technology, China, and the used male Kunming rats (8-week-old; 300–320 g) were purchased from Shanxi Medical University, China.

The rats were firstly premedicated by general anesthesia. Then, a cylindrical sample ($d1.5 \text{ mm} \times 3 \text{ mm}$) infected with *S. mutans* was implanted in the tibia of rats. Finally, muscle fasciae and skin were carefully sutured and closed. Half the rats were euthanized 3 d after surgery. The implants were taken out, and then the survived bacteria in the soft tissues around the implants were separated. The spread plate method was used to evaluate the in vivo antibacterial activity. 4 weeks after surgery, the femurs with the samples of the remaining rats were harvested after euthanasia and were inspected by a micro-CT (VivoCT80, Scanco Medical, Switzerland) to observe the newly formed bone. The in vivo biological safety was also studied by staining the heart, liver, spleen, lung, and kidney with hematoxylin and eosin (H&E) staining.

2.6 Statistical analysis

All experiments were performed at least three times and the data were expressed as mean \pm standard deviation (SD). A one-way analysis of variance (ANOVA) and a Student–Newman–Keuls (SNK) post hoc test were applied to determining the statistical significance by using SPSS 14.0 ($p < 0.001$ was considered to be extremely significant).

3 Results and discussion

3.1 Sample characterization

The microstructure of the prepared GQDs was observed by TEM (Figs. 1(a) and (b)). The average diameter of GQDs was about 15 nm, and the lattice distance of 0.325 nm corresponded to the (002) crystallographic facet of graphitic carbon [35]. The surface topography of TiO₂ NR is shown in Fig. 1(c). Uniform nanorods with a mean rod diameter of 45 nm were observed on Ti. G-TiO₂ NR was further prepared by the second hydrothermal treatment of TiO₂ NR in a GQDs-containing solution. As shown in Fig. 1(d), compared with TiO₂ NR, the diameter of the G-TiO₂ NR increased because of the increase in reaction time [36]. Figure 1(e) shows the TEM image of the G-TiO₂ nanorod with a mean diameter of 60 nm. The lattice distance of 0.36 nm was observed from the (101) plane of TiO₂ (Fig. 1(f)), and the incorporation of GQDs did not change the phase. The AFM images of Ti, TiO₂ NR and G-TiO₂ NR are shown in

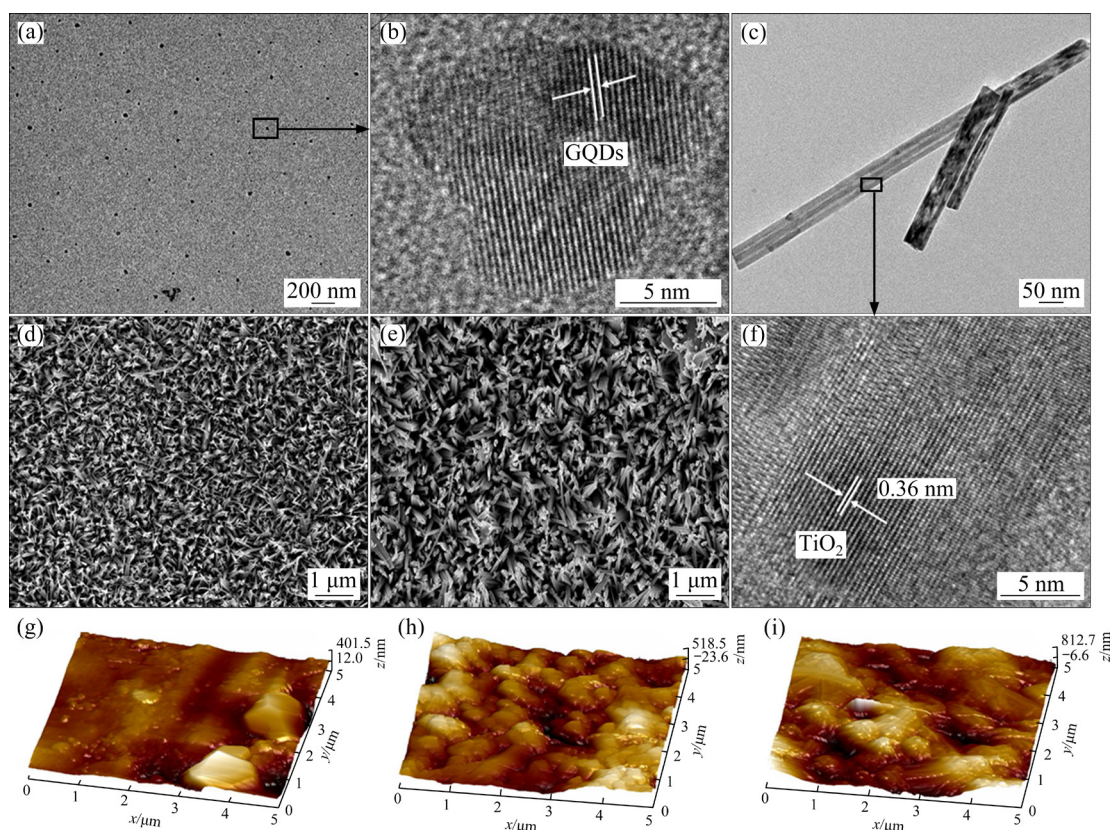


Fig. 1 TEM (a) and HR-TEM (b) images of GQDs, SEM images of TiO₂ NR (c) and G-TiO₂ NR (d), TEM (e) and HR-TEM (f) images of G-TiO₂ NR, and AFM images of Ti (g), TiO₂ NR (h) and G-TiO₂ NR (i)

Figs. 1(g–i). The roughness of G-TiO₂ NR was slightly greater than that of TiO₂ NR.

The XRD patterns of GQDs, TiO₂ and G-TiO₂ NRs are shown in Fig. 2(a). The TiO₂ phase in both TiO₂ and G-TiO₂ NRs mainly consisted of anatase and no significant difference was found. A broad peak in the pattern of GQDs was ascribed to the (002) plane of graphitic carbon. No feature peaks of GQDs were observed in G-TiO₂ NR owing to the low content in the TiO₂. XPS was performed to determine the chemical states of G-TiO₂ and shown in Fig. 2(b), compared to the spectrum of TiO₂ NR, the intensity of C 1s and N 1s in that of the G-TiO₂ NR increased significantly. The C 1s spectrum detected from G-TiO₂ (Fig. 2(c)) was fitted with four peaks centered at 284.30, 284.85, 285.66 and 288.10 eV that were attributed to C–C, C–N, C–O and C=O, respectively [37]. The O 1s spectrum of G-TiO₂ (Fig. 2(d)) showed three peaks at 529.39, 530.13 and 531.54 eV, which were assigned to Ti–O–Ti, C=O and C–O–H, respectively [38]. The XPS characterization confirmed that GQDs were successfully doped in TiO₂ NR. The FTIR spectra of GQDs, TiO₂

and G-TiO₂ NRs are shown in Fig. 2(e). The characteristic absorption of GQDs could be observed in the spectrum of G-TiO₂ NR, further demonstrating that TiO₂ NR was modified with GQDs. Figure 2(f) illustrates the surface wettability of various samples. The contact angle of Ti was about 53°, while the value decreased to 9.1° on TiO₂ NR owing to the changes in the surface morphology and free energy [39]. The doping of GQDs did not change the wettability significantly.

3.2 In vitro antibacterial property

The antibacterial activity of TiO₂ and G-TiO₂ NRs against *S. mutans* was evaluated by the spread plate method and fluorescent staining, respectively. As shown in Figs. 3 and 4, after incubation for 24 h, there was some decrease in the number of bacterial colonies on TiO₂ NR compared with Ti, and the antibacterial efficiency was about 25%, meaning that the nanorod structure of TiO₂ NR exhibited a certain antibacterial activity. However, only several bacterial colonies were observed on G-TiO₂ NR, and the antibacterial efficiency reached 97.8%, which suggested that the doping of GQDs made the

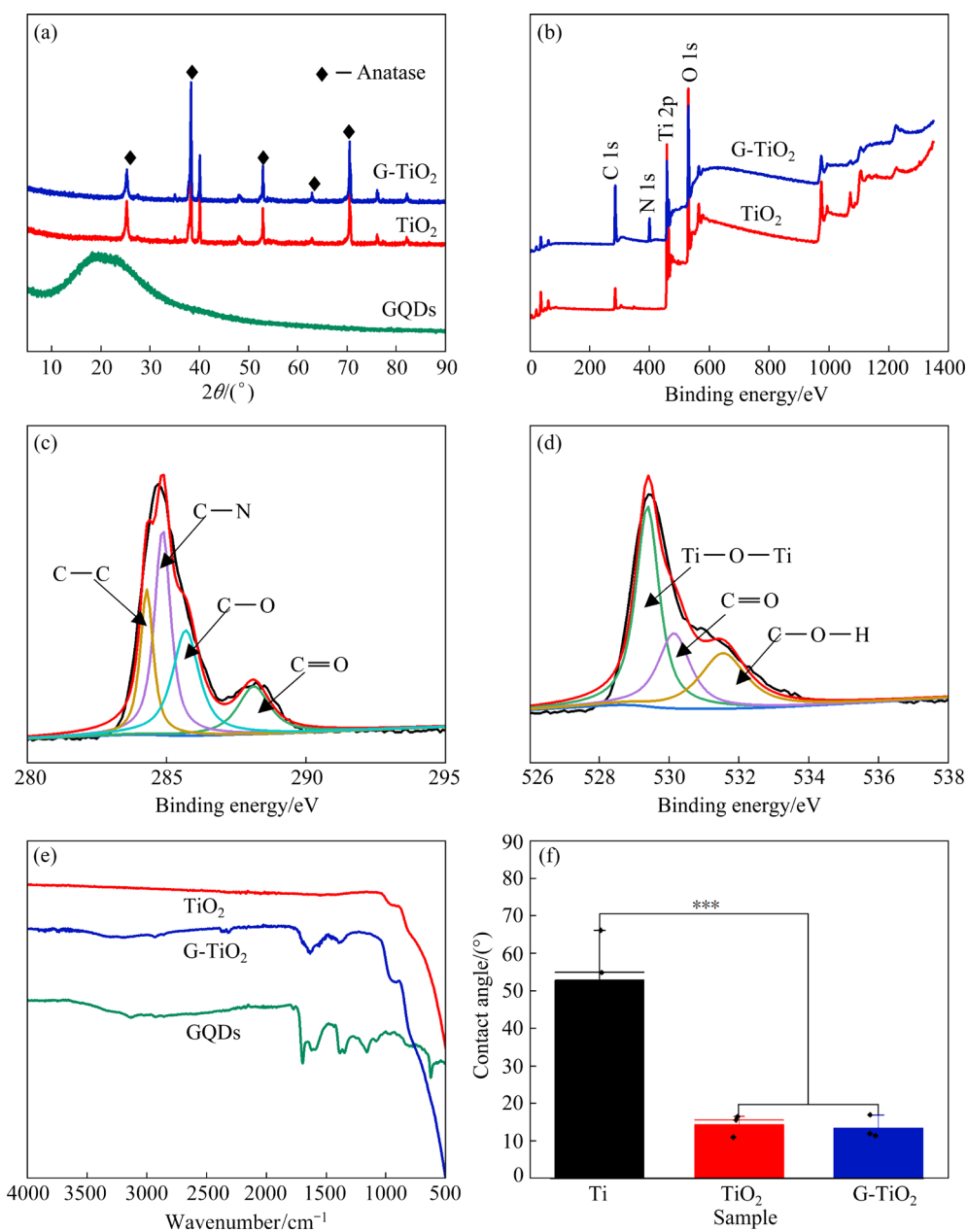


Fig. 2 XRD patterns of GQDs, TiO₂ and G-TiO₂ NRs (a), XPS survey spectra (b), high-resolution spectra of C 1s (c) and O 1s (d) of G-TiO₂ NR, FTIR spectra of GQDs, TiO₂ and G-TiO₂ NRs (e), and contact angle of Ti, TiO₂ NR and G-TiO₂ NR (f) (***) $p < 0.001$)

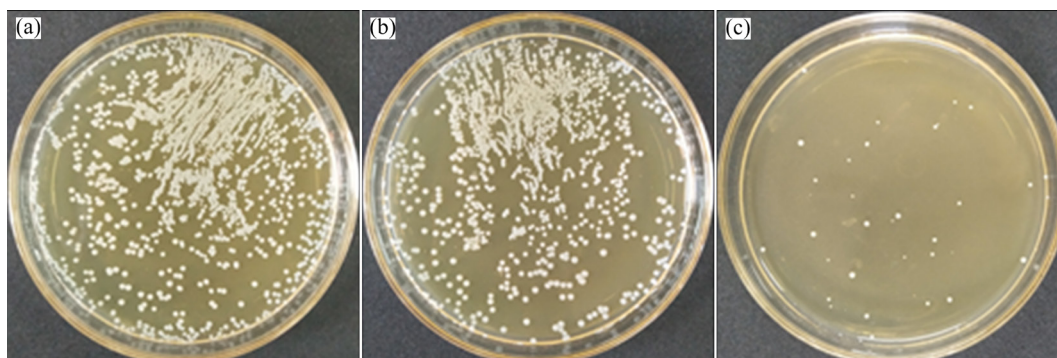


Fig. 3 Photographs of *S. mutans* colonies on surface of Ti (a), TiO₂ NR (b) and G-TiO₂ NR (c)

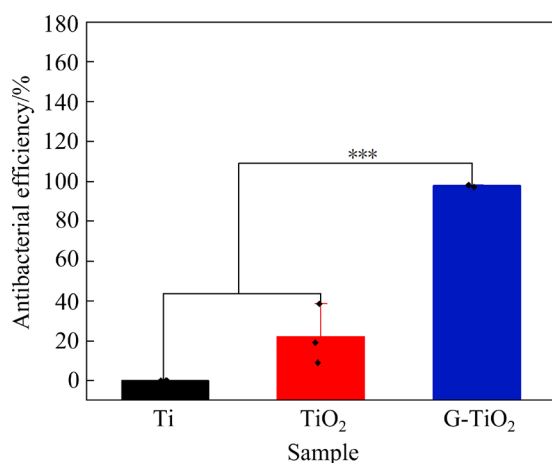


Fig. 4 Antibacterial efficiency of Ti, TiO₂ NR and G-TiO₂ NR (***p* < 0.001)

G-TiO₂ NR possess excellent antibacterial activity. The results of live/dead (green/red) fluorescence staining are shown in Fig. 5. The surfaces of Ti and TiO₂ NR were stained with green, indicating that most of the bacteria survived. In contrast, only several green spots were found on the surface of G-TiO₂ NR, further demonstrating the excellent antibacterial property.

The antibacterial mechanism of G-TiO₂ NR has two aspects: (1) histidine functionalized GQDs; (2) physical puncture by the nanorods. It is generally known that graphene-based nanomaterials possess antibacterial activity because they can disrupt the integrity of bacterial cell membrane [40]. In this work, the synthesized GQDs were functionalized with imidazolyl which also has antibacterial activity [41,42]. It has also been reported that the nanostructures on the surface of implants can kill bacteria by physico-mechanical interactions, and the nanorod structure exhibits the strongest antibacterial activity among the nanostructures [12,18]. In addition, the zeta potentials of GQDs and G-TiO₂ NR were about 8.4 and 7.8 mV, respectively. As is well known, bacteria are negatively charged. Thus, G-TiO₂ NR can capture bacterial by electrostatic adsorption and then the combined actions of GQDs functionalized with histidine and puncturing by the TiO₂ nanorods disrupt the cell membranes, causing bacterial death.

3.3 Biocompatibility

Figure 6 shows the cell morphology and

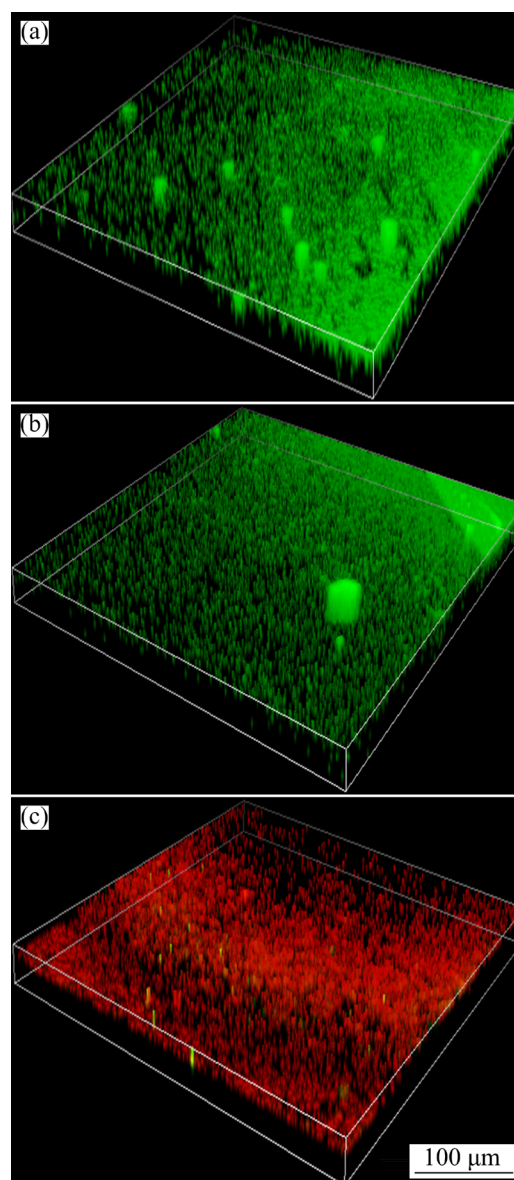


Fig. 5 Live/dead fluorescence images of *S. mutans* on surface of Ti (a), TiO₂ NR (b) and G-TiO₂ NR (c)

spreading of BMSCs after culture for 24 h on Ti, TiO₂ NR and G-TiO₂ NR. The BMSCs were elongated and spread poorly on pristine Ti. However, spreading of cells on TiO₂ NR was better and polygonal shape with filamentous pseudopodia could be found. As is well known, the nanostructure on the surface of implants can improve the adhesion, spreading, and differentiation of BMSCs, which is mediated by cell alignment of the cytoskeleton and formation of focal adhesions [43,44]. There were no significant changes in cellular morphology between TiO₂ and G-TiO₂ NRs, suggesting that the introduction of GQDs has no obvious effect on the biocompatibility of TiO₂ NR.

3.4 In vivo antibacterial assay and osteogenic activity

To evaluate the in vivo antibacterial activity and new bone formation of G-TiO₂ NR, an animal model with *S. mutans* infection in the tibia of rats was established, and pristine Ti was used as the control. After feeding for 3 d, half the rats were euthanized, and the implants were removed. The residual bacteria in the soft tissues around the

implants were separated ultrasonically and cultured for in vivo antibacterial evaluation by spread plate method. The results are shown in Fig. 7. A lot of bacterial colonies were observed in the medium corresponding to pristine Ti implant, while only several colonies could be found in the medium corresponding to G-TiO₂ NR, which indicated that G-TiO₂ NR exhibited excellent in vivo antibacterial activity.

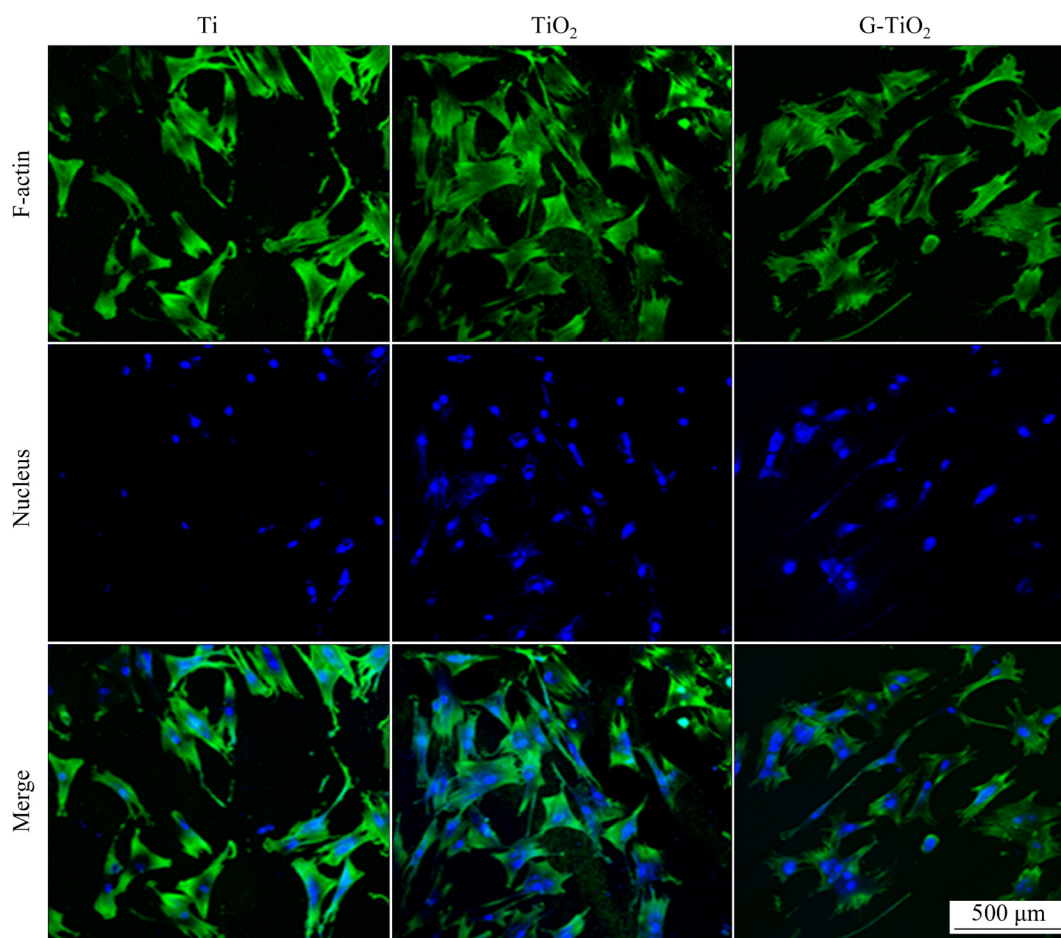


Fig. 6 Fluorescence images of BMSCs cultured on Ti, TiO₂ NR and G-TiO₂ NR for 24 h

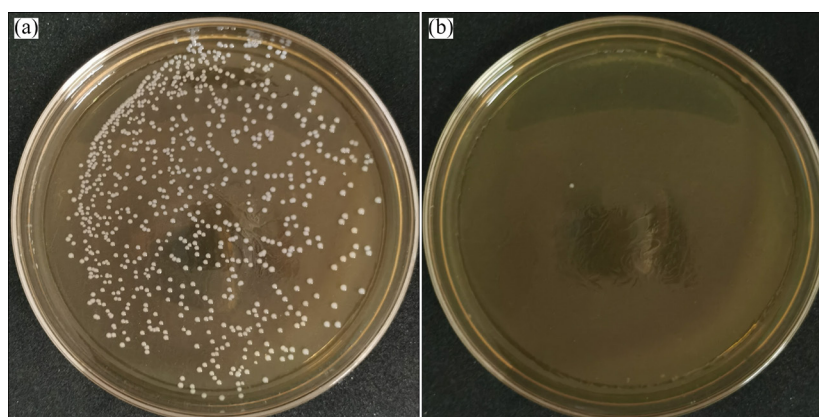


Fig. 7 Photographs of bacteria colonies of Ti (a) and G-TiO₂ NR (b)

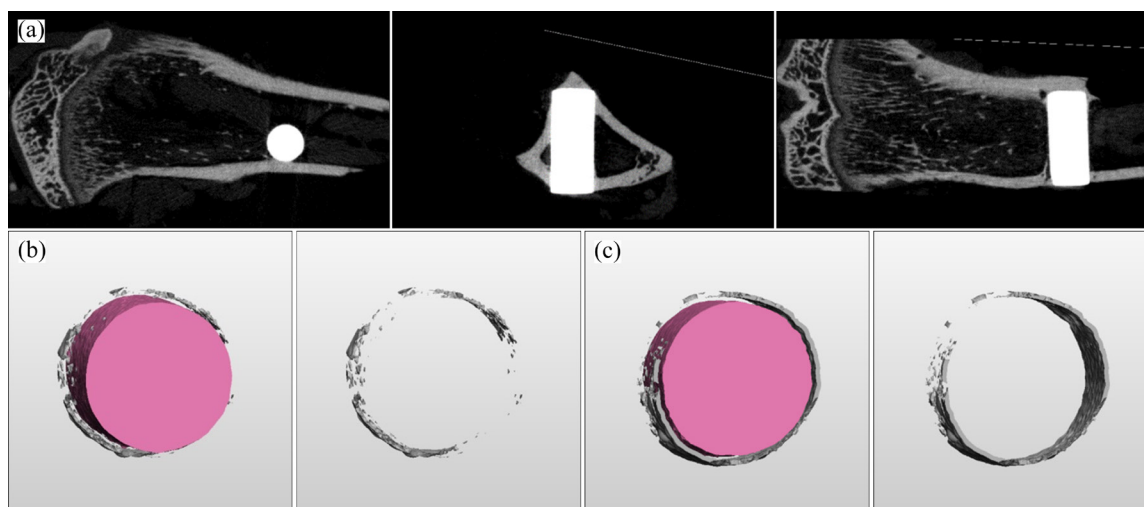


Fig. 8 2D micro-CT images of G-TiO₂ NR in tibia (a), and 3D images reconstructed by micro-CT in Ti (b) and G-TiO₂ NR (c) implants

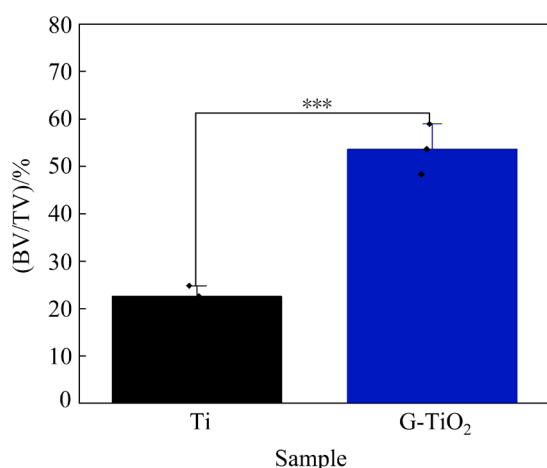


Fig. 9 Quantitative analysis of BV/TV (***) $p < 0.001$)

After being fed for four weeks of the remained rats, the newly formed bone on the surface of *S. mutans* infected Ti and G-TiO₂ NR implants was monitored by micro-CT. Figure 8(a) shows the 2D micro-CT images of G-TiO₂ NR implant in tibia from different directions. 3D-reconstructed images (Figs. 8(b) and (c)) show that new bone mass around G-TiO₂ NR was much larger than that of the pristine Ti implant, and the corresponding bone/tissue volume ratio (BV/TV) of Ti and G-TiO₂ NR was 22.64% and 53.62%, respectively (Fig. 9). The results indicate that G-TiO₂ NR could promote new bone formation effectively even in the presence of infection.

The biological safety of G-TiO₂ NR in vivo was also evaluated by H&E staining of major organs, as shown in Fig. 10, no obvious abnormalities

were observed in the heart, liver, spleen, lung and kidney of rats, suggesting that G-TiO₂ NR did not produce side effects on rats.

4 Conclusions

(1) GQDs-modified TiO₂ NR was successfully prepared on Ti to improve the antibacterial activity and long-term osseointegration ability. The mean diameter of the nanorod was 60 nm, and the NR significantly improved the hydrophilicity of Ti.

(2) G-TiO₂ NR exhibited excellent antibacterial activity in vitro and in vivo due to the synergistic effect of GQDs and physical puncturing by the nanorod. On the other hand, G-TiO₂ NR showed good biocompatibility to promote BMSCs spreading and new bone formation. This study provided an innovative strategy for the surface design of Ti dental implants to address the implant-associated infections.

Acknowledgments

This work was financially supported by the National Natural Science Foundation of China (Nos. 52171240, 81902273), the Postdoctoral Science Foundation of China (No. 2021M691992), the Major Projects in Research and Development of Shanxi Province, China (Projects of International Cooperation, No. 201803D421090) and the Natural Science Foundation of Special Equipment Safety Supervision Inspection Institute of Jiangsu Province, China (No. KJ(Y)2020037).

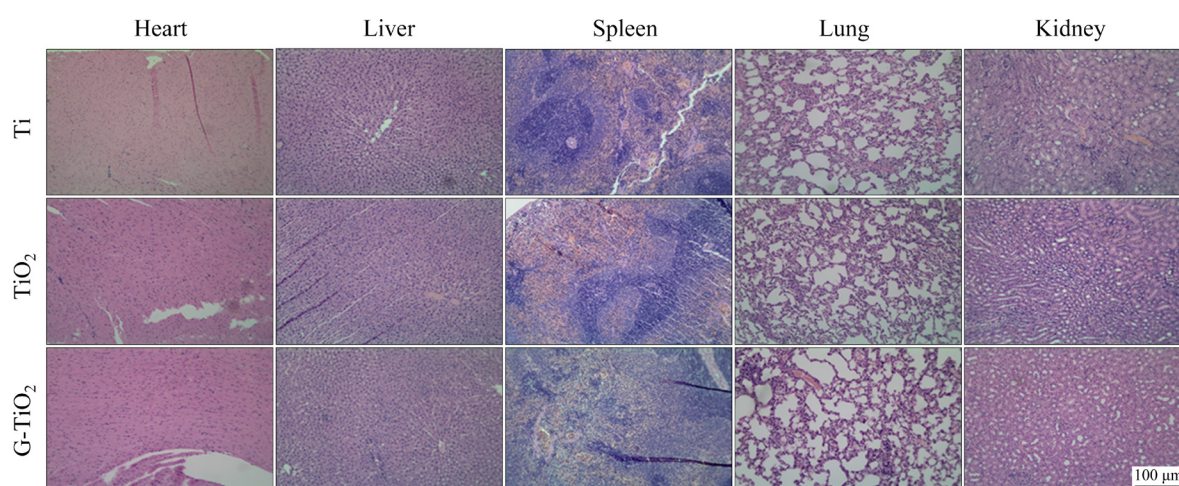


Fig. 10 H&E staining of major organ tissue slides

References

- [1] BAUER S, SCHMUKI P, MARK K V D, PARK J. Engineering biocompatible implant surfaces. Part I: Materials and surfaces [J]. *Progress in Materials Science*, 2013, 58: 261–326.
- [2] SITI NUR HAZWANI M R, LIM L X, LOCKMAN Z, ZUHAILAWATI H. Fabrication of titanium-based alloys with bioactive surface oxide layer as biomedical implants: Opportunity and challenges [J]. *Transactions of Nonferrous Metals Society of China*, 2022, 32: 1–44.
- [3] MISHNAEVSKY L J, LEVASHOV E, VALIEV R Z, SEGURADO J, SABIROV I, ENIKEEV N, PROKOSHKIN S, SOLOV'YOV A V, KOROTITSKIY A, GUTMANAS E, GOTMAN I, RABKIN E, PSAKH'E S, DLUHOŠ L, SEEFELDT M, SMOLIN A. Nanostructured titanium-based materials for medical implants: Modeling and development [J]. *Materials Science and Engineering R*, 2014, 81: 1–19.
- [4] CHAI Mao-zhou, AN Mei-wen, ZHANG Xiang-yu. Construction of a $\text{TiO}_2/\text{MoSe}_2/\text{CHI}$ coating on dental implants for combating *Streptococcus mutans* infection [J]. *Materials Science and Engineering C*, 2021, 129: 112416.
- [5] VYAS N, GREWAL M, KUEHNE S A, SAMMONS R L, WALMSLEY A D. High speed imaging of biofilm removal from a dental implant model using ultrasonic cavitation [J]. *Dental Materials*, 2020, 36: 733–743.
- [6] KALELKAR P P, RIDDICK M, GARCLÁ A J. Biomaterial-based antimicrobial therapies for the treatment of bacterial infections [J]. *Nature Reviews Materials*, 2021, 7: 39–54.
- [7] CHUA Song-lin, YAM J K H, HAO Pi-liang, ADAV S S, SALIDO M M, LIU Yang, GIVSKOV M, SZE S, TOLKER-NIELSEN T, YANG Liang. Selective labelling and eradication of antibiotic-tolerant bacterial populations in *Seudomonas aeruginosa* biofilms [J]. *Nature Communications*, 2016, 7: 10750.
- [8] LIU Yong, BUSSCHER H J, ZHAO Bing-ran, LI Yuan-feng, ZHANG Zhen-kun, MEI H C, REN Yi-jin, SHI Lin-qi. Surface-adaptive, antimicrobially loaded, micellar nano-carriers with enhanced penetration and killing efficiency in staphylococcal biofilms [J]. *ACS Nano*, 2016, 10: 4779–4789.
- [9] GAO Ang, HANG Rui-qiang, HUANG Xiao-bo, ZHAO Ling-zhou, ZHANG Xiang-yu, WANG Lin, TANG Bin, MA Sheng-li, CHU P K. The effects of titania nanotubes with embedded silver oxide nanoparticles on bacteria and osteoblasts [J]. *Biomaterials*, 2014, 35: 4223–4235.
- [10] ZHANG Xiang-yu, WU Hai-bo, GENG Zhen-hua, HUANG Xiao-bo, HANG Rui-qiang, MA Yong, YAO Xiao-hong, TANG Bin. Microstructure and cytotoxicity evaluation of duplex-treated silver-containing antibacterial TiO_2 coatings [J]. *Materials Science and Engineering C*, 2014, 45: 402–410.
- [11] QIN Hui, CAO Hui-liang, ZHAO Yao-chao, ZHU Cheng, CHENG Tao, WANG Qiao-jie, PENG Xiao-chun, CHENG Meng-qi, WANG Jia-xin, JIN Guo-dong, JIANG Yao, ZHANG Xian-long, LIU Xuan-yong, CHU P K. In vitro and in vivo anti-biofilm effects of silver nanoparticles immobilized on titanium [J]. *Biomaterials*, 2014, 35: 9114–9125.
- [12] ZHANG Xiang-yu, ZHANG Guan-nan, CHAI Mao-zhou, YAO Xiao-hong, CHEN Wei-yi, CHU P K. Synergistic antibacterial activity of physical-chemical multi-mechanism by TiO_2 nanorod arrays for safe biofilm eradication on implant [J]. *Bioactive Materials*, 2021, 6: 12–25.
- [13] WU Shui-lin, WENG Zheng-yang, LIU Xiang-mei, YEUNG K W K, CHU P K. Functionalized TiO_2 based nanomaterials for biomedical applications [J]. *Advanced Functional Materials*, 2014, 24: 5464–5481.
- [14] MODARESIFAR K, AZIZIAN S, GANJIAN M, FRATILA-APACHITEI L E, ZADPOOR A A. Bactericidal effects of nanopatterns: A systematic review [J]. *Acta Biomaterialia*, 2019, 83: 29–36.
- [15] YAVARI S A, CASTENMILLER S M, STRIJP J A G, CROES M. Combating implant infections: Shifting focus from bacteria to host [J]. *Advanced Materials*, 2020, 32: 2002962.
- [16] TAN Lei, LI Jun, LIU Xiang-mei, CUI Zhen-duo, YANG Xian-jin, ZHU Shen-li, LI Zhao-yang, YUAN Xu-bo,

- ZHENG Yu-feng, YEUNG K W K, PAN Hao-bo, WANG Xian-bao, WU Shui-lin. Rapid biofilm eradication on bone implants using red phosphorus and near-infrared light [J]. *Advanced Materials*, 2018, 30: 1801808.
- [17] XIE Xian-zhou, MAO Cong-yang, LIU Xiang-mei, TAN Lei, CUI Zhen-duo, YANG Xian-jin, ZHU Sheng-li, LI Zhao-yang, YUAN Xu-bo, ZHENG Yu-feng, YEUNG K W K, CHU P K, WU Shui-lin. Tuning the bandgap of photo-sensitive polydopamine/Ag₃PO₄/graphene oxide coating for rapid, noninvasive disinfection of implants [J]. *ACS Central Science*, 2018, 4: 724–738.
- [18] ZHANG Guan-nan, YANG Yong-qiang, SHI Jing, YAO Xiao-hong, CHEN Wei-yi, WEI Xiao-chun, ZHANG Xiang-yu, CHU P K. Near-infrared light II-assisted rapid biofilm elimination platform for bone implants at mild temperature [J]. *Biomaterials*, 2021, 269: 120634.
- [19] MAO Cong-yang, XIANG Yi-ming, LIU Xiang-mei, CUI Zhen-duo, YANG Xian-jin, LI Zhao-yang, ZHU Sheng-li, ZHENG Yu-feng, YEUNG K W K, WU Shui-lin. Repeatable photodynamic therapy with triggered signaling pathways of fibroblast cell proliferation and differentiation to promote bacteria-accompanied wound healing [J]. *ACS Nano*, 2018, 12: 1747–1759.
- [20] XIANG Yi-ming, ZHOU Qi-lin, LI Zhao-yang, CUI Zhen-duo, LIU Xiang-mei, LIANG Yan-qin, ZHU Sheng-li, ZHENG Yu-feng, YEUNG K W K, WU Shui-lin. A Z-scheme heterojunction of ZnO/CDots/C₃N₄ for strengthened photoresponsive bacteria-killing and acceleration of wound healing [J]. *Journal of Materials Science & Technology*, 2020, 57: 1–11.
- [21] ANSARI M O, KALAMEGAM G, ESSA A, BENCHERIF S A, MEMIC A. Graphene and graphene-based materials in biomedical applications [J]. *Current Medicinal Chemistry*, 2019, 26: 6834–6850.
- [22] YANG Yu-qi, ASIRI A M, TANG Zhi-wen, DU Dan, LIN Yue-he. Graphene based materials for biomedical applications [J]. *Materials Today*, 2013, 16: 365–373.
- [23] GURUNATHAN S, KIM J H. Synthesis, toxicity, biocompatibility, and biomedical applications of graphene and graphene-related materials [J]. *International Journal of Nanomedicine*, 2016, 11: 1927–1945.
- [24] SANTOS C M, TRIA M C R, VERGARA R A M V, AHMED F, ADVINCULA R C, RODRIGUES D F. Antimicrobial graphene polymer (PVK-GO) nanocomposite films [J]. *Chemical Communications*, 2011, 47: 8892–8894.
- [25] DELLIEU L, LAWARÉE E, RECKINGER N, DIDEMBOURG C, LETESSON J J, SARRAZIN M, DEPARIS O, MATROULE J Y, COLOMER J F. Do CVD grown graphene films have antibacterial activity on metallic substrates? [J]. *Carbon*, 2015, 84: 310–316.
- [26] QIU Jia-jun, GUO Jing-shu, GENG Hao, QIAN Wen-hao, LIU Xuan-yong. Three-dimensional porous graphene nanosheets synthesized on the titanium surface for osteogenic differentiation of rat bone mesenchymal stem cells [J]. *Carbon*, 2017, 125: 227–235.
- [27] ZHOU Kai, YU Peng, SHI Xiao-jun, LING Ting-xian, ZENG Wei-nan, CHEN An-jing, YANG Wei, ZHOU Zong-ke. Hierarchically porous hydroxyapatite hybrid scaffold incorporated with reduced graphene oxide for rapid bone ingrowth and repair [J]. *ACS Nano*, 2019, 13: 9595–9606.
- [28] ZHOU Xiao-yan, LI Rui-yi, LI Zai-jun, GU Zhi-guo, WANG Guang-li. Ultrafast synthesis of gold/proline-functionalized graphene quantum dots and its use for ultrasensitive electrochemical detection of *p*-acetamidophenol [J]. *RSC Advances*, 2016, 6: 42751–42755.
- [29] CHEN Wei, LI Rui-yi, LI Zai-jun, YANG Yong-qiang, ZHU Hai-yan, LIU Jun-kang. Promising copper oxide–histidine functionalized graphene quantum dots hybrid for electrochemical detection of hydroquinone [J]. *Journal of Alloys and Compounds*, 2019, 777: 1001–1009.
- [30] YANG Hong-wei, YU Meng, WANG Rong, LI Bo, ZHAO Xin, HAO Yu-lin, GUO Zheng, HAN Yong. Hydrothermally grown TiO₂-nanorods on surface mechanical attrition treated Ti: Improved corrosion fatigue and osteogenesis [J]. *Acta Biomaterialia*, 2020, 116: 400–414.
- [31] ZHANG Guan-nan, ZHANG Xing-yu, YANG Yong-qiang, CHI Rui-fang, SHI Jing, HANG Rui-qing, HUANG Xiao-bo, CHU P K, ZHANG Xiang-yu. Dual light-induced in situ antibacterial activities of biocompatible TiO₂/MoS₂/PDA/RGD nanorod arrays on titanium [J]. *Biomaterials Science*, 2020, 8: 391–404.
- [32] LI Xue-yuan, ZHANG Yang, QI Guo-xian. Evaluation of isolation methods and culture conditions for rat bone marrow mesenchymal stem cells [J]. *Cytotechnology*, 2013, 65: 323–334.
- [33] BAI Long, CHEN Pei-ru, ZHAO Ya, HANG Rui-yue, YAO Xiao-hong, TANG Bin, LIU Chang-sheng, XIAO Yin, HANG Rui-qiang. A micro/nano-biomimetic coating on titanium orchestrates osteo/angio-genesis and osteo-immunomodulation for advanced osseointegration [J]. *Biomaterials*, 2021, 278: 121162.
- [34] HE Dong-mei, ZHANG Xiang-yu, YAO Xiao-hong, YANG Yong-qiang. In vitro and in vivo highly effective antibacterial activity of carbon dots-modified TiO₂ nanorod arrays on titanium [J]. *Colloids and Surfaces B: Biointerfaces*, 2022, 211: 112318.
- [35] DHAR S, MAJUMDER T, MONDAL S P. Graphene quantum dot-sensitized ZnO nanorod/polymer schottky junction UV detector with superior external quantum efficiency, detectivity, and responsivity [J]. *ACS Applied Materials & Interfaces*, 2016, 8: 31822–31831.
- [36] ZHANG Guan-nan, ZHANG Xing-yu, YANG Yong-qiang, ZHANG Hong-yu, SHI Jing, YAO Xiao-hong, ZHANG Xiang-yu. Near-infrared light-triggered therapy to combat bacterial biofilm infections by MoSe₂/TiO₂ nanorod arrays on bone implants [J]. *Advanced Materials Interface*, 2020, 7: 1901706.
- [37] LIN Li-ping, SONG Xin-hong, CHEN Yi-ying, RONG Ming-cong, ZHAO Ting-ting, JIANG Ya-qi, WANG Yi-ru, CHEN Xi. One-pot synthesis of highly greenish-yellow fluorescent nitrogen-doped graphene quantum dots for pyrophosphate sensing via competitive coordination with Eu³⁺ ions [J]. *Nanoscale*, 2015, 7: 15427–15433.
- [38] YAN Xiao, LI Yan-juan, LI Ma-lin, JIN Yong-cheng, DU Fei, CHEN Gang, WEI Ying-jin. Ultrafast lithium storage in TiO₂-bronze nanowires/N-doped graphene nanocomposites [J]. *Journal of Materials Chemistry A*, 2015, 3: 4180–4187.

- [39] FENG Xin-jian, FENG Lin, JIN Mei-hua, ZHAI Jin, JIANG Lei, ZHU Dao-ben. Reversible super-hydrophobicity to super-hydrophilicity transition of aligned ZnO nanorod films [J]. *Journal of the American Chemical Society*, 2004, 126: 62–63.
- [40] RADHI A, MOHAMAD D, RAHMAN F S A, ABDULLAH A M, HASAN H. Mechanism and factors influence of graphene-based nanomaterials antimicrobial activities and application in dentistry [J]. *Journal of Materials Research and Technology*, 2021, 11: 1290–1307.
- [41] RAMACHANDRAN R, RANI M, SENTHAN S, JEONG Y T, KABILAN S. Synthesis, spectral, crystal structure and in vitro antimicrobial evaluation of imidazole/benzotriazole substituted piperidin-4-one derivatives [J]. *European Journal of Medicinal Chemistry*, 2011, 46: 1926–1934.
- [42] WANG Pei-yi, WANG Ming-wei, ZENG Dan, XIANG Meng, RAO Jia-rui, LIU Qing-qing, LIU Li-wei, WU Zhi-bing, LI Zhong, SONG Bao-an, YANG Song. Rational optimization and action mechanism of novel imidazole (or imidazolium)-labeled 1,3,4-oxadiazole thioethers as promising antibacterial agents against plant bacterial diseases [J]. *Journal of Agricultural and Food Chemistry*, 2019, 67: 3535–3545.
- [43] GITTENS R A, OLIVARES-NAVARRETE R, SCHWARTZ Z, BOYAN B D. Implant osseointegration and the role of microroughness and nanostructures: Lessons for spine implants [J]. *Acta Biomaterialia*, 2014, 10: 3363–3371.
- [44] LIU Xue-li, WANG Shu-tao. Three-dimensional nano-biointerface as a new platform for guiding cell fate [J]. *Chemical Society Reviews*, 2014, 43: 2385–2401.

钛种植体表面石墨烯量子点改性 二氧化钛纳米棒阵列的抗菌性能

张翔宇¹, 鲁舒心², 赫东梅², 柴茂洲¹, 武壮壮³, 姚晓红², 杨永强⁴

1. 太原理工大学 生物医学工程学院, 太原 030024;
2. 太原理工大学 材料科学与工程学院 医用金属材料山西省重点实验室, 太原 030024;
3. 山西医科大学 第二附属医院 骨科 骨与软组织损伤修复山西省重点实验室, 太原 030001;
4. 国家石墨烯产品质量检验检测中心(江苏) 江苏省特种设备安全监督检验研究院, 无锡 214174

摘要: 为防止植入体细菌感染, 通过水热法在钛种植体表面制备石墨烯量子点掺杂的 TiO₂ 纳米棒阵列。采用扫描电子显微镜、高分辨透射电子显微镜、原子力显微镜、X 射线光电子能谱仪、X 射线衍射仪和傅里叶转换红外光谱仪对纳米棒阵列进行表征, 证明石墨烯量子点被成功掺杂到 TiO₂ 纳米棒表面, 纳米棒平均直径为 60 nm, 且纳米棒阵列的亲水性能得到明显改善。由于石墨烯量子点与纳米棒结构的协同作用, 掺杂纳米棒阵列对变异链球菌表现出优良的抗菌能力, 其抗菌率为 97.8%。此外, 掺杂纳米棒阵列还具有良好的生物相容性及成骨性能, 在感染模型下依然可以促进新骨生成。

关键词: 石墨烯量子点; 纳米棒; 钛; 抗菌性能; 骨整合

(Edited by Wei-ping CHEN)